

Recognition of Single-Point Mutation Using a Biological Nanopore

Ping Liu and Ryuji Kawano*

Here the recognition of a single-point mutation in oligonucleotides is described by using nanopore measurements. The translocation behavior of a series of mutated DNA strands, hybridized with a complementary DNA probe, is analyzed via blocking current and unzipping time. Discernment of the mutation position at the single nucleotide level is achieved by analysis of a 2D graph of the bootstrapped translocation data. The proposed approach provides a useful tool for the mutation detection of oligonucleotides secreted from tumor cells and is applicable in simple and label-free diagnoses as a nanopore liquid biopsy.

1. Introduction

Liquid biopsy is a recently emerging approach for cancer diagnosis.^[1] Tumor-related biomaterials such as DNA and RNA fragments, in addition to whole cancer cells, are released from tumors into bodily fluids. For instance, circulating tumor cells (CTCs) that circulate in the bloodstream contain detectable information about the parent tumor cell.^[2] On the other hand, circulating tumor DNA (ctDNA) or microRNA (miRNA) also have genetic information relating to the tumor cells.^[3,4] These short fragments of nucleic acids are usually encapsulated in extracellular vesicles or bound to proteins and circulate in the blood. Diagnosis via ctDNA detection is particularly common for cancers such as lung cancer.^[5–7] The epidermal growth factor receptor (EGFR) gene, which is a component of the molecular signaling pathway that controls the proliferation and growth of cells, is the most crucial driver oncogene of lung cancer. Namely, the mutation of L858R and T790M in EGFR is expressed in patients with non-small-cell lung cancer. Liquid biopsy of ctDNA from the bloodstream can be used to detect this mutation and for the subsequent diagnosis of lung cancer.^[8] Current methods to assess the mutation of ctDNA include digital polymerase chain reaction and next-generation sequencing (NGS).^[9] These measurements require multiple procedures and are often time-consuming. Considering the relatively short half-life of ctDNA sampled from blood (several

minutes to several tens of minutes),^[10,11] a more rapid detection method could offer improved diagnostic performance.

Nanopore technology^[12–16] is a promising candidate for the rapid detection of mutated ctDNAs. There are two different nanopore approaches for liquid biopsy: nanopore sequencing of ctDNA or direct sensing of ctDNA using a nanopore. Nanopore sequencing has recently emerged as a rapid and inexpensive method of DNA sequencing.^[17] Nanopore sequencing is capable of recognizing a small difference

in ionic current when an single-stranded DNA (ssDNA) passes through the nanopore under an applied voltage. Advantages of such sequencing include the use of compact bench-top instruments and the capacity for long read. While there have previously been many applications of nanopore sequencing focusing on genome sequencing, the analysis of ctDNA has remained a challenge. On the other hand, nanopore sensing is able to directly detect the translocation of short DNA strands via the blocking current of the open-pore state.^[18] Regarding the point mutation analysis of short DNA using nanopore sensing, several approaches have been reported, including using an enzyme reaction,^[19] nanolock,^[20] DNA nanopore,^[21] or probe DNA.^[22,23] Although these methods can determine the presence or absence of a single mutation, prediction of the mutation position has remained challenging.

We have previously developed single molecular detection methods using nanopores,^[24–31] including analysis of the unzipping time of double-stranded DNA and RNA with bootstrapping.^[14,29] Hiratani and Kawano applied nanopore decoding of DNA computing outputs for miRNA pattern recognition.^[29] Two miRNAs that are overexpressed and secreted from tumor cells were recognized via diagnostic DNA (dgDNA) hybridization, with formation of a four-way junction in the presence of both miRNAs. Nanopore measurements were able to decode translocation behavior to discriminate the four AND operations: (0,0) in the absence of either miRNA; (0,1) and (1,0) in the presence of a single miRNA; and (1,1) demonstrating the unzipping pattern of the four-way junction in the presence of both miRNAs. Bootstrapping of the data offered significant improvement in distinguishing between all four systems in cases where the raw duration data had been unable to distinguish any differences. The unzipping analysis has widely used not only the oligonucleotides but also protein unfolding.^[32–34]

In this study, discernment of the position of the single-point mutation in oligonucleotides was achieved by analysis of unzipping behavior in a method analogous to that of Hiratani's work.^[29] The target oligonucleotides (21 nt) based on an EGFR sequence were hybridized with probe DNA to form a double-stranded


P. Liu

Department of Food and Energy Systems Science
Tokyo University of Agriculture and Technology
Tokyo 184-8588, Japan

Prof. R. Kawano

Department of Biotechnology and Life Science
Tokyo University of Agriculture and Technology
Tokyo 184-8588, Japan

E-mail: rjkawano@cc.tuat.ac.jp

 The ORCID identification number(s) for the author(s) of this article can be found under <https://doi.org/10.1002/smt.202000101>.

DOI: 10.1002/smt.202000101

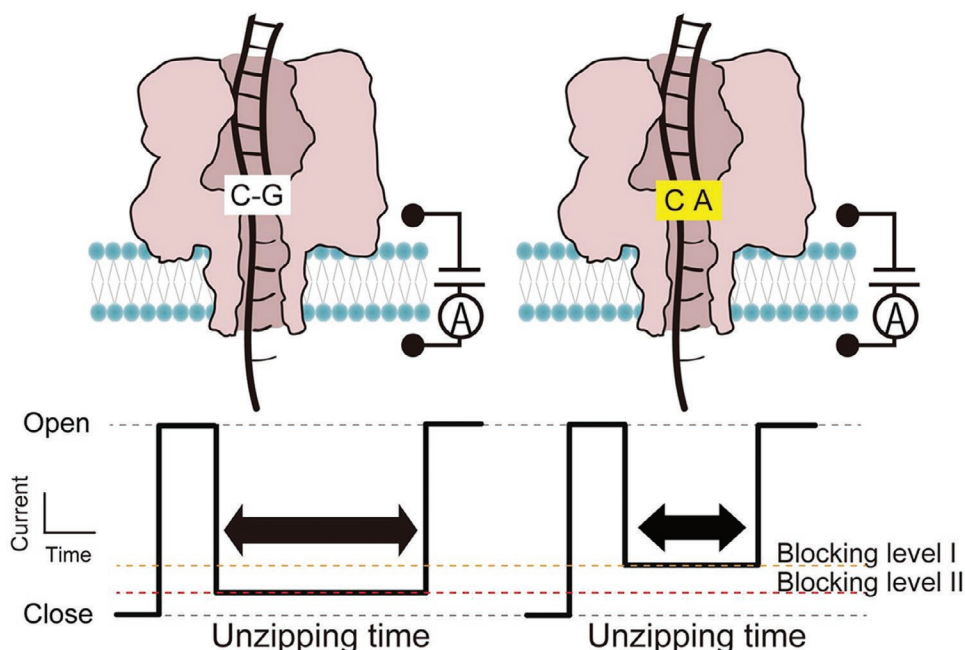


Figure 1. Illustration of the unzipping technique for detection of mutation position in target nucleotides by combining the analysis of blocking level and unzipping time.

complex with a polynucleotide tail. The mutation position in target nucleotides was detected by the analysis of bootstrapped data of the blocking ratio and duration time of unzipping events (Figure 1).

Our approach offers a useful tool for the rapid and label-free detection of mutation positions not only in ctDNA but also in a wide variety of oligonucleotides.

2. Results

2.1. The Design of the Complementary Probe for the Target Oligonucleotides

The target sequence used in this study relates to the Exon21 region of the EGFR. To facilitate detection of this target, two DNA probes were prepared. The P5T probe consisted of the complementary sequence, with the target poly(deoxyadenylic acid) 30-mers sequence (poly(dA)₃₀) at the 5' terminus, while the P3T probe had this positioned at the 3' terminus. poly(dA)₃₀ is sufficiently long to extend in one instance from the *cis* to the *trans* side of the alpha-hemolysin (α HL) pore, and hence ensures the capturing of double-stranded DNA (dsDNA) in the nanopore. Regarding the target DNAs, five sequences were designed that had a single-point mutation from (C–G) to (C–A) at five different positions, named G1A, G2A, G3A, G11A, and G21A, respectively. Besides, the nucleotide variation from (C–G) to (C–A), (C–T), and (C–C) at the terminus was also investigated, in targets named G1A, G1T, and G1C. All sequences used in this study are listed in Table 1.

2.2. Detection of Point-Mutation Position Using the P5T Probe

Figure 2a–e shows the typical current and time traces of the unzipping events using P5T with G1A, G11A, and G21A

under application of +120 mV voltage. In the case of the P5T probe itself (ssP5T, Figure 2a), rapid translocation events were observed. In contrast, longer blocking durations for the hybridized complexes (Figure 2b–e) indicate the unzipping events between the target and P5T probe in the nanopore. Although the blocking ratio of the three mutated DNA targets was less than that of the wild-type (WT) system, the difference was too small for discrimination between these mutants. On the other hand, the unzipping time is shown to be exponentially dependent upon the Gibbs free energy (ΔG) of the hybridization, as simulated by Nucleic Acid Package (NUPACK) (Figure 2f). However, significant overlap in the histograms of unzipping time (Figure 2g) led to difficulty in distinguishing between mutation positions. It can be further seen that overlapping data remain in the clusters of plot data even when combining the blocking duration and unzipping time (Figure 2g). Hence, although use of the P5T probe was able to demonstrate differences in measured parameters,

Table 1. Sequences of probe DNA and target DNA.

Name	Sequence
P5T	5'-(A) ₃₀ CCCTTGACGACAGCAGTTCCTCC-3'
P3T	5'-CCCTTGACGACAGCAGTTCCTCC(A) ₃₀ -3'
Wild	5'-GGGAAGCTGCTGTCGTC AAGGG-3'
G1A	5'-AGGAAGCTGCTGTCGTC AAGGG-3'
G2A	5'-GAGGAAGCTGCTGTCGTC AAGGG-3'
G3A	5'-GGAAGCTGCTGTCGTC AAGGG-3'
G11A	5'-GGGAAGCTGCTATCGTC AAGGG-3'
G21A	5'-GGGAAGCTGCTGTCGTC AAGGA-3'
G1T	5'-TGGAAGCTGCTGTCGTC AAGGG-3'
G1C	5'-CGGAAGCTGCTGTCGTC AAGGG-3'

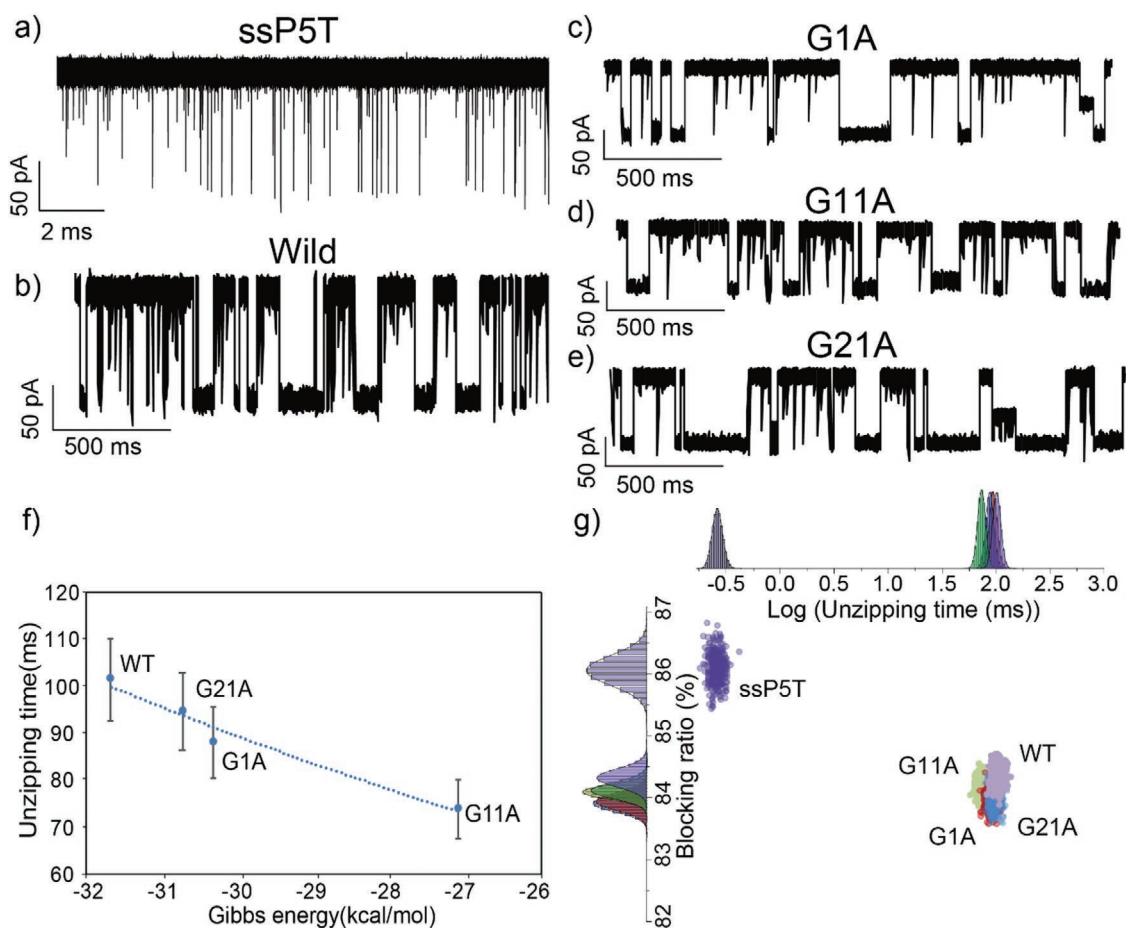


Figure 2. Results when using P5T for the detection of mutation position. Typical current traces of P5T hybridized to a) ssP5T, b) wild-type, c) G1A, d) G11A, and e) G21A. f) Unzipping time as a function of the simulated hybridization energy calculated using NUPACK. g) Scatter plot of unzipping time versus blocking ratio.

it was unable to offer precise discrimination of mutation positions.

2.3. Detection of Point-Mutation Position Using the P3T Probe

Enhanced distinguishability between data clusters for each DNA target was achieved by changing the complementary probe from P5T to P3T. In the case of the P3T–WT hybridized complex, the unzipping time increased significantly from 38 ± 4 to 587 ± 60 ms, and the blocking ratio also increased from 84% to 89% (Figure 3a). Reasons for this are proposed in the “Discussion” section. Figure 3b presents the scatter plots of the blocking ratio and unzipping time of the unzipping events of the WT and five different mutants hybridized with P3T. The order of the blocking ratio is shown to be WT > G1A > G11A > G21A. It is notable that this order was also demonstrable in the series where the positions of mutated nucleotide were in high proximity: WT > G1A > G2A > G3A. On the other hand, the unzipping time did not show such a clear tendency with mutation position. It has previously been reported that the unzipping time has correlation with the ΔG of hybridization.^[35,36] Our results support this hypothesis, as evident in Figure 3c, in which there is a remarkably clear relationship between unzipping time and ΔG of hybridization.

2.4. Different Mismatched Pairs at the Same Mutation Position

The capacity to recognize varied nucleotide mutations at the same position for G1A, G1C, G1T, and WT was also tested. During unzipping initiation, this position is closest to the constricted region of the α HL pore (Figure 4a). The order of blocking and unzipping times was WT > G1A \approx G1C > G1T and WT \gg G1A > G1T > G1C, respectively. Although each parameter was individually insufficient for discernment of the mutated nucleotide, the data points for a given mutant and for the WT can be seen to lie in distinct regions of the scatter plot shown in Figure 4b. However, the ΔG of hybridization in this case did not have correlation with the unzipping time (Figure 4c).

3. Discussion

3.1. Differences between the P5T and P3T Probes

In the case of B-form DNA, molecular modeling demonstrates that dsDNA overstretched from the 3' ends is more stable against force-induced dehybridization than that from the

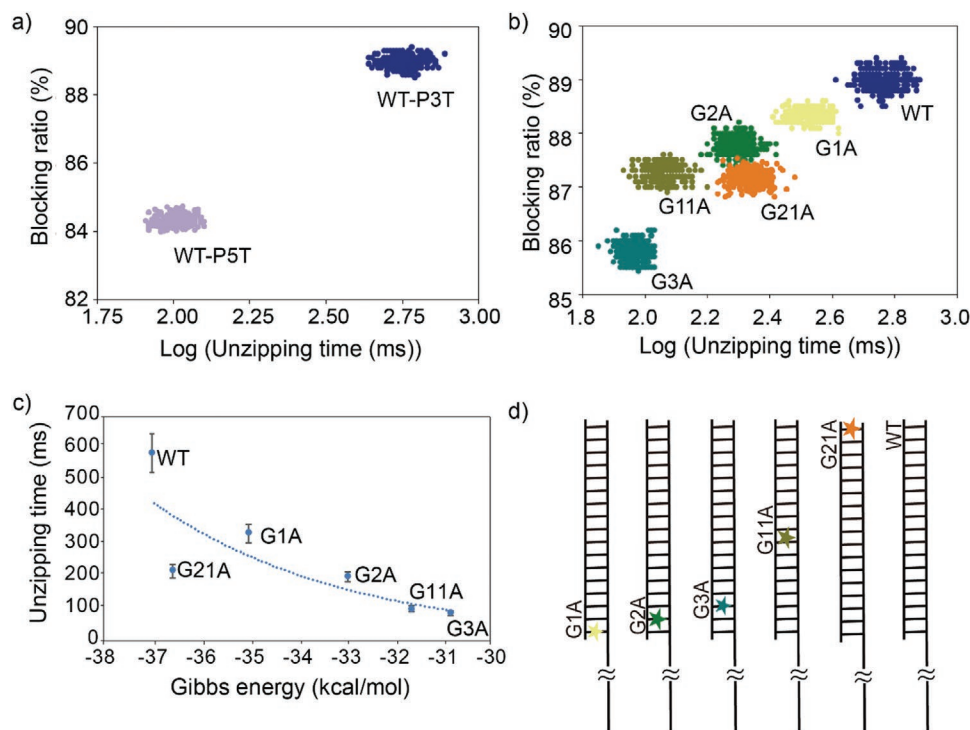


Figure 3. Results when using P3T for the detection of mutation positions. a) Positioning the poly(dA)₃₀ at the 3' terminal shows increased unzipping time and blocking ratio relative to P5T. b) Scatter plots of the blocking ratio and unzipping time of five different mutation patterns and the wild-type, each hybridized with P3T. c) Unzipping time versus simulated ΔG of hybridization. The dotted line shows to guide the eye. d) Diagram showing mutation positions.

5'5' ends.^[37] This behavior causes differing geometry for these two cases under axial extension as studied in magnetic bead experiments; extension from the 3' ends leads to a flat ribbon conformation while extension from the 5' ends leads to a narrow fiber with a strongly negatively inclined base. The pulling forces for the 3'3' and 5'5' ends are 141 ± 3 and 122 ± 4 pN, respectively, demonstrating that the 3'3' ends are 15% more stable than the 5'5' ends. Similar behavior occurs in nanopore unzipping events (Figure 5a,b). The mean unzipping times of P5T (5'5') and P3T (3'3') were 101 ± 9 and 587 ± 61 ms, respectively, revealing that the P3T (3'3') system has an unzipping time of over five times slower. Although the length of dsDNA and the experimental conditions in this study differed

to the previously reported magnetic bead experiment, the trend in stability of P3T (stable) > P5T (unstable) was mostly consistent with the previous results.^[38]

3.2. Trends in Blocking Ratio in the P3T System

The level of current blocking in the mutant-P3T system is seen to be much lower than that of the WT system. It is proposed that increased flexibility of the unpaired bases offers a reduced barrier to ion mobility, and therefore a lower reduction in current. The blocking level is dependent upon mutation position, with the order of the blocking ratio following WT > G1A > G2A > G3A.

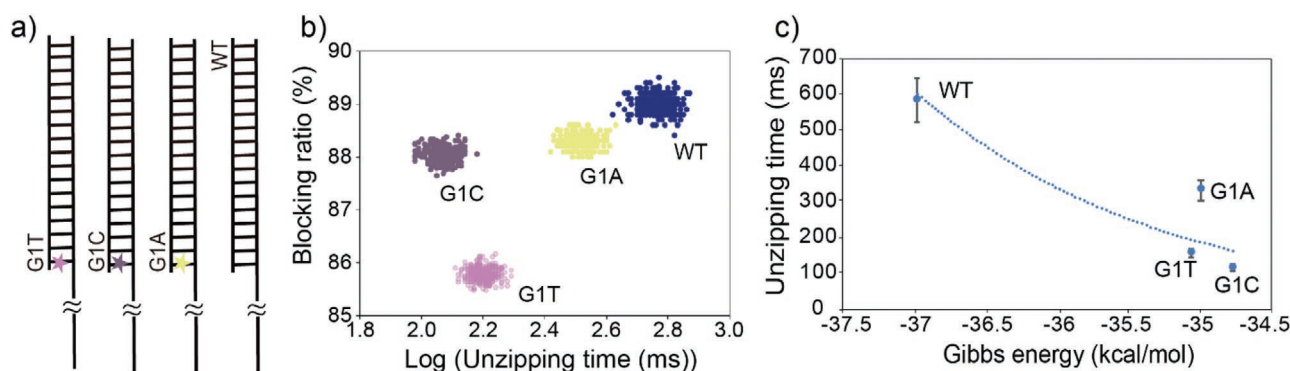


Figure 4. Results when using P3T for the detection of different mismatched pairs at the same position. a) Diagram showing different mismatched pairs at the same position. b) Scatter plots of different mismatch patterns in the same position. c) Unzipping time versus simulated ΔG of hybridization. The dotted line shows to guide the eye.

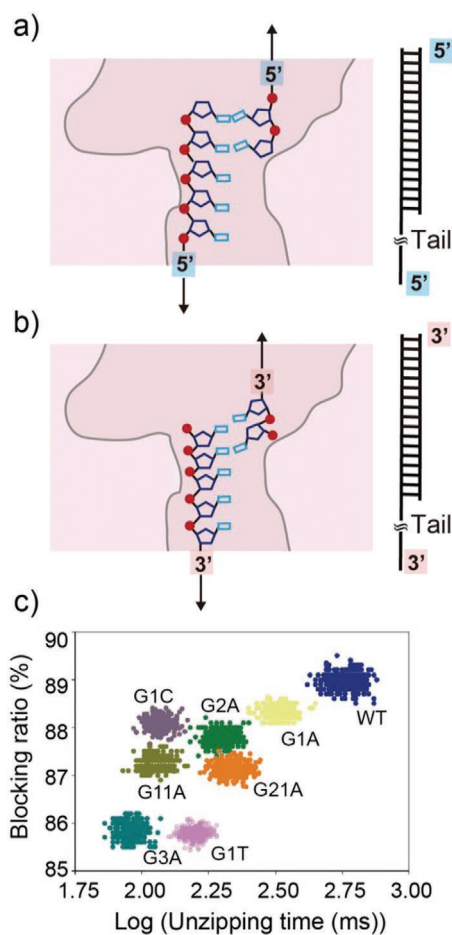


Figure 5. a) Diagram demonstrating the unzipping conformation of the 5'5' double-stranded DNA–P5T hybrid in an α HL pore. b) Diagram demonstrating the unzipping conformation of the 3'3' double-stranded DNA–P3T hybrid in an α HL pore. c) Scatter plots showing the combined result of both mutation at differing position, and mutation at the same position but to differing nucleotides.

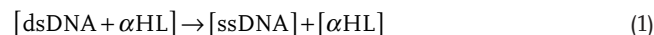
This pattern demonstrates that a reduced ion current flows when the mutation position is further from the constricted region of the α HL nanopore during unzipping. It can be explained that due to the short strand length of two or fewer nucleotides (G3A, G2A, and G1A) below the mutated site, only weak hydrogen bonding of these bases occurs. Thermodynamic simulations with NUPACK at 25 °C, the same DNA concentration in the channel current measurements (1×10^{-6} M) has been set, support this assumption (Figure S1, Supporting Information). While in the unzipping conformation, these weakly bound bases are less able to restrict ion mobility than in dsDNA where the mutation lies further from the constricted pore site. In such cases where mutations are further from the limiting aperture in α HL during unzipping, the ordering showed inconsistencies. For instance, the blocking ratio of G11A was higher than that of G3A although the position of G11A is further from the constricted site than G3A. This result may indicate that G3A presents a minimum blocking level, with any mutation above G3A having a similar blocking ratio.

In the GxC and GxT mutants, the order of the blocking ratio was WT > G1C \approx G1A > G1T. Reasons for this trend are proposed

to follow the above trend for the GxA system, in which the flexible base effect causes a reduction in current blocking ratio. The effect of base identity on the blocking ratio (G1C \approx G1A > G1T) highlighted herein may be further explained based on a previous study concerning the interaction between the hairpin DNA (hpDNA) terminus and the α HL pore wall.^[39,40] The ten base pair hpDNA with a T-overhang (10 bp•T) was shown to have a low activation energy, indicating that there is a weak interaction between the T-overhang and the restricted region of the α HL nanopore. The T-terminal mutant therefore is proposed to have a more flexible terminus which is less able to impair ion mobility.

3.3. Trends in Unzipping Time in the P3T System

The unzipping time is shown to be dependent upon the ΔG within the same mutation group (GxA). This result is consistent with the previous studies.^[35,36] It has been previously discussed that the unzipping kinetics of dsDNA through the nanopore follows the first-order reaction as follows



The rate constant of this reaction can be described as below

$$k = k_0 \exp(-\Delta G_{\text{sim}} / k_B T) \quad (2)$$

$$k = 1 / t \quad (3)$$

where k is the dissociation rate constant, k_0 is the initial rate constant, ΔG_{sim} is the simulated ΔG , k_B is the Boltzmann constant used for the single-molecule study, T is the temperature, and t is the peak value of unzipping time histogram after bootstrapping. Unzipping data of the GxA series were fitted using Equation (2) as shown in Figure S2 (Supporting Information). Equation (2) was well fitted and this result suggests the first-order reaction even in the mutation system. On the other hand, the mutation series such as GxT and GxC did not fit well using an exponential curve (Figure 4c). This result may imply that there is a unique relationship between the ΔG and the unzipping time in each mutation series.

4. Conclusion

A method for the detection of single-point mutation in oligonucleotides using nanopore measurement was developed. Conventional nanopore measurements use two parameters to analyze molecule detection: the blocking current and the duration time of molecular translocation through the nanopore. In the case of conventional detection of mutated oligonucleotides, the translocation speed of the oligonucleotides is too rapid to recognize the mutation. In this study, translocation speed is slowed by using a hybridized probe on the target nucleotides. Bootstrapping was applied for a more precise analysis of the unzipping time, which was shown to exhibit the correlation with the hybridization energy predicted by thermodynamic simulations. By optimization of the DNA probe, discrimination of mutation position at the single-nucleotide resolution was

achieved. Furthermore, mutant variations such as GxA, GxC, and GxT are also discernible using the method described. By plotting the blocking ratio against unzipping time, it shown to be possible to distinguish between mutants. Our method offers a powerful tool for the mutation detection for oligonucleotides and is proposed to be applicable for simple cancer diagnosis using ctDNA as a nanopore liquid biopsy.

5. Experimental Section

Reagents and Chemicals: In this study, the following reagents were used: 1,2-diphytanoyl-*sn*-glycero-3-phosphocholine (DPhPC; Avanti Polar Lipids, Alabaster, AL, USA), *n*-decane (Wako Pure Chemical Industries, Ltd., Osaka, Japan), potassium chloride (KCl; Nacalai Tesque), Buffered electrolyte solutions were prepared from ultrapure water, which was obtained from a Milli-Q system (Millipore, Billerica, MA, USA). α HL (Sigma-Aldrich, St. Louis, MO, USA) was obtained as a monomer protein isolated from *Staphylococcus aureus* in the form of a powder, dissolved at a concentration of 1 mg mL⁻¹ in 1 M KCl, and stored at -80 °C. For use, samples were diluted to 600 × 10⁻⁹ M using a buffered electrolyte solution and stored at 4 °C. Each DNA (Eurofins Genomics K.K., Japan) was obtained from DNA synthesis in the form of a powder, dissolved at a concentration of 100 × 10⁻⁶ M in ultrapure water, and stored at -20 °C.

Design and Formation of the Probes and Mutated DNA: The free energies of P3T and P5T with mutated DNA were calculated by thermodynamic simulations using NUPACK web-server.^[41] Annealing of the double strands was conducted by heating a DNA sample for 5 min at 50 × 10⁻⁶ M in ultrapure water at 95 °C and gradually cooling to room temperature.

Bilayer Lipid Membrane Preparation and Reconstitution of α -Hemolysin: Bilayer lipid membranes (BLMs) were prepared using a device produced by microfabrication (Figure S3a, Supporting Information). The method of fabrication was previously reported.^[26,42,43] BLMs can be formed in this device by the droplet contact method (Figure S3b, Supporting Information). First, the DPhPC (lipids/*n*-decane, 10 mg mL⁻¹) solution (0.6 μ L) was dropped into each chamber. Second, the buffer solution (1 M KCl, 10 × 10⁻³ M 3-(*N*-morpholino)propane sulfonic acid, pH 7.0, and 5 μ L) with α HL and DNA (final concentration = 1 × 10⁻⁶ M) was dropped into each chamber. A few minutes after adding the buffer solution, the two lipid monolayers combined to form BLMs. α HL formed nanopores by insertion in the BLM. Upon rupture of BLMs, they were reformed by manual agitation between two chambers with a hydrophobic stick.^[44]

Channel Current Measurements and Data Analysis: The channel current was monitored using an Axopatch 200B amplifier (Molecular Devices, USA), filtered with a low-pass Bessel filter at 10 kHz at a sampling rate of 50 kHz. A constant voltage of +120 mV was applied from the *trans* side, with the *cis* side was grounded. Recorded data were acquired with Clampex 9.0 software (Molecular Devices, USA) through a Digidata 1440A analog-to-digital converter (Molecular Devices, USA). Data were analyzed using Clampfit 10.7 (Molecular Devices, USA), Excel (Microsoft, Washington, USA), and Python (Python Software Foundation, Delaware, USA). The analyzed data were chosen from over three different α HL nanopores. DNA translocation event was defined at inhibition of >80% of open α HL channel current. The blocking ratios were calculated with the open and blocking channel conductance. Unzipping time was filtered between 7 and 12 000 ms. The bootstrap method is based on the resampling of the original random sample drawn from a population with an unknown distribution. The exact bootstrap method, which availed the entire space of resamples, was used. In the exact bootstrap method, the verification of accuracy will be made possible when the sample number is over 30.^[45] In this work, this bootstrap procedure took 300 samples randomly from the primary common logarithmic translocation data with 65 536 replacements and to calculate the means for these samples. The bootstrapped data produced the histograms and plots of logarithmic unzipping time and blocking ratios. The error bars shown in Figures 2f,

3c, and 4c were the widths of two standard deviations after bootstrapping (68.27% of the data fall within one standard deviation of the mean).

Supporting Information

Supporting Information is available from the Wiley Online Library or from the author.

Acknowledgements

This work was partly supported by KAKENHI (Grant Nos. 17K19138 and 19H00901) from MEXT, Japan. With thanks to K. Shimizu, A. Tamotsu, M. Yamaji, and A. Cooney for useful discussions on data analysis and for language editing.

Conflict of Interest

The authors declare no conflict of interest.

Keywords

circulating-tumor DNA, liquid biopsy, nanopore sensing, single-point mutation

Received: February 12, 2020

Revised: June 18, 2020

Published online:

- [1] E. Crowley, F. Di Nicolantonio, F. Loupakis, A. Bardelli, *Nat. Rev. Clin. Oncol.* **2013**, *10*, 472.
- [2] M. Yu, S. Stott, M. Toner, S. Maheswaran, D. A. Haber, *J. Cell Biol.* **2011**, *192*, 373.
- [3] J. Hayes, P. P. Peruzzi, S. Lawler, *Trends Mol. Med.* **2014**, *20*, 460.
- [4] H. Schwarzenbach, D. S. B. Hoon, K. Pantel, *Nat. Rev. Cancer* **2011**, *11*, 426.
- [5] C. C. Lin, W. L. Huang, F. Wei, W. C. Su, D. T. Wong, *Expert Rev. Mol. Diagn.* **2015**, *15*, 1427.
- [6] T. Jiang, S. X. Ren, C. C. Zhou, *Lung Cancer* **2015**, *90*, 128.
- [7] C. Alix-Panabieres, K. Pantel, *Cancer Discovery* **2016**, *6*, 479.
- [8] L. A. Diaz, A. Bardelli, *J. Clin. Oncol.* **2014**, *32*, 579.
- [9] G. Perkins, H. Lu, F. Garlan, V. Taly, *Adv. Clin. Chem.* **2017**, *79*, 43.
- [10] F. Diehl, M. Li, D. Dressman, Y. P. He, D. Shen, S. Szabo, L. A. Diaz, S. N. Goodman, K. A. David, H. Juhl, K. W. Kinzler, B. Vogelstein, *Proc. Natl. Acad. Sci. USA* **2005**, *102*, 16368.
- [11] Y. M. D. Lo, J. Zhang, T. N. Leung, T. K. Lau, A. M. Z. Chang, N. M. Hjelm, *Am. J. Hum. Genet.* **1999**, *64*, 218.
- [12] J. J. Kasianowicz, E. Brandin, D. Branton, D. W. Deamer, *Proc. Natl. Acad. Sci. USA* **1996**, *93*, 13770.
- [13] C. Cao, Y. T. Long, *Acc. Chem. Res.* **2018**, *51*, 331.
- [14] R. Kawano, *Biotechnol. J.* **2018**, *13*, 1800091.
- [15] Y. Wang, D. Zheng, Q. Tan, M. X. Wang, L. Q. Gu, *Nat. Nanotechnol.* **2011**, *6*, 668.
- [16] K. Tian, Z. He, Y. Wang, S. J. Chen, L. Q. Gu, *ACS Nano* **2013**, *7*, 3962.
- [17] A. Ameur, W. P. Kloosterman, M. S. Hestand, *Trends Biotechnol.* **2019**, *37*, 72.
- [18] D. W. Deamer, D. Branton, *Acc. Chem. Res.* **2002**, *35*, 817.
- [19] X. H. Chen, G. M. Roozbahani, Z. J. Ye, Y. W. Zhang, R. Ma, J. L. Xiang, X. Y. Guan, *ACS Appl. Mater. Interfaces* **2018**, *10*, 11519.
- [20] Y. Wang, K. Tian, R. C. Shi, A. Gu, M. Pennella, L. Alberts, K. S. Gates, G. F. Li, H. X. Fan, M. X. Wang, L. Q. Gu, *ACS Sens.* **2017**, *2*, 975.

- [21] S. Howorka, S. Cheley, H. Bayley, *Nat. Biotechnol.* **2001**, *19*, 636.
- [22] Q. F. Yang, T. T. Ai, Y. Lv, Y. Q. Huang, J. Geng, D. Xiao, C. S. Zhou, *Anal. Chem.* **2018**, *90*, 8102.
- [23] F. J. Yao, Y. N. Zhang, Y. F. Wei, X. F. Kang, *Chem. Commun.* **2014**, *50*, 13853.
- [24] R. Kawano, T. Osaki, H. Sasaki, M. Takinoue, S. Yoshizawa, S. Takeuchi, *J. Am. Chem. Soc.* **2011**, *133*, 8474.
- [25] M. Hiratani, M. Ohara, R. Kawano, *Anal. Chem.* **2017**, *89*, 2312.
- [26] M. Ohara, M. Takinoue, R. Kawano, *ACS Synth. Biol.* **2017**, *6*, 1427.
- [27] H. Watanabe, A. Gubbiotti, M. Chinappi, N. Takai, K. Tanaka, K. Tsumoto, R. Kawano, *Anal. Chem.* **2017**, *89*, 11269.
- [28] H. L. Zhang, M. Hiratani, K. Nagaoka, R. Kawano, *Nanoscale* **2017**, *9*, 16124.
- [29] M. Hiratani, R. Kawano, *Anal. Chem.* **2018**, *90*, 8531.
- [30] K. Shoji, R. Kawano, R. J. White, *ACS Nano* **2019**, *13*, 2606.
- [31] M. Matsushita, K. Shoji, N. Takai, R. Kawano, *J. Phys. Chem. B* **2020**, *124*, 2410.
- [32] D. Rodriguez-Larrea, H. Bayley, *Nat. Nanotechnol.* **2013**, *8*, 288.
- [33] E. L. Bonome, F. Cecconi, M. Chinappi, *Nanoscale* **2019**, *11*, 9920.
- [34] L. Mereuta, A. Asandei, I. Schiopu, Y. Park, T. Luchian, *Anal. Chem.* **2019**, *91*, 8630.
- [35] A. F. Sauer-Budge, J. A. Nyamwanda, D. K. Lubensky, D. Branton, *Phys. Rev. Lett.* **2003**, *90*, 238101.
- [36] M. Ohara, Y. Sekiya, R. Kawano, *Electrochemistry* **2016**, *84*, 338.
- [37] C. Danilowicz, C. Limouse, K. Hatch, A. Conover, V. W. Coljee, N. Kleckner, M. Prentiss, *Proc. Natl. Acad. Sci. USA* **2009**, *106*, 13196.
- [38] A. Lebrun, R. Lavery, *Nucleic Acids Res.* **1996**, *24*, 2260.
- [39] V. S. DeGuzman, C. C. Lee, D. W. Deamer, W. A. Vercoutere, *Nucleic Acids Res.* **2006**, *34*, 6425.
- [40] W. A. Vercoutere, S. Winters-Hilt, V. S. DeGuzman, D. Deamer, S. E. Ridino, J. T. Rodgers, H. E. Olsen, A. Marziali, M. Akeson, *Nucleic Acids Res.* **2003**, *31*, 1311.
- [41] J. N. Zadeh, C. D. Steenberg, J. S. Bois, B. R. Wolfe, M. B. Pierce, A. R. Khan, R. M. Dirks, N. A. Pierce, *J. Comput. Chem.* **2011**, *32*, 170.
- [42] R. Kawano, Y. Tsuji, K. Sato, T. Osaki, K. Kamiya, M. Hirano, T. Ide, N. Miki, S. Takeuchi, *Sci. Rep.* **2013**, *3*, 1995.
- [43] R. Kawano, *ChemPhysChem* **2018**, *19*, 359.
- [44] R. Kawano, Y. Tsuji, K. Kamiya, T. Kodama, T. Osaki, N. Miki, S. Takeuchi, *PLoS One* **2014**, *9*, e102427.
- [45] J. Kisielinska, *Comput. Stat.* **2013**, *28*, 1061.